Micromechanical model of weakly-cemented sediments

Ran Holtzman

Original citation & hyperlink:
Holtzman, R. "Micromechanical model of weakly-cemented sediments." *International Journal for Numerical and Analytical Methods in Geomechanics* 36.7 (2012): 944-958.
https://dx.doi.org/10.1002/nag.2078

ISSN 0363-9061
ESSN 1096-9853

Publisher: Wiley

Micromechanical model of weakly-cemented sediments

R. Holtzman*

Department of Soil and Water Sciences, The Hebrew University of Jerusalem, P.O. Box 12, Rehovot 76100, Israel

SUMMARY

Experiments indicate that the bulk stiffness of weakly-cemented granular materials increases significantly with the applied load, a nonlinearity which is not captured by most micromechanical models. Here, we study the deformation of weakly-cemented materials through grain-scale simulations. We show that the frequently-made assumption of linear-elastic cement and intergranular contact area which varies according to a Hertzian-type model cannot explain the observed nonlinearity of the bulk response. We introduce the micromechanical effect of mechanisms such as closure and opening of microcracks, granular cement and material heterogeneity through an effective contact stiffness which depends on the local deformation. We find that an exponential dependence between the effective stiffness and the local deformation, with a high exponent value, provides bulk stiffness which is in good agreement with experimental data. The inability of models with weaker intergranular stiffness-deformation dependence to reproduce the experimental data demonstrates the highly-nonlinear nature of the intergranular deformation. Our results highlight the importance of accounting for grain-scale mechanisms in modeling granular materials, and provide a plausible explanation for the nonlinear behavior of weakly-cemented sediments.

Received ...

KEY WORDS: nonlinear deformation; grain-scale simulations; intergranular slip; Hertz contact; macroscopic elastic moduli; bulk stiffness

1. INTRODUCTION

In weakly-cemented granular materials, particles are bonded together by small amounts of cement. Cementation of the intergranular contacts of a particulate material, even by relatively soft cement, significantly enhances its bulk stiffness [1]. In sediments and rocks, preferential cementation at the grain contacts can occur by deposition of minerals in aqueous solution which infiltrates the sediment at low fluid saturations [1], or by pressure dissolution of the grain material [2]. Understanding the mechanics of weakly-cemented materials is both scientifically challenging and important in many practical applications. For instance, poorly-consolidated sedimentary rocks are often associated with subsidence, borehole instability, and sanding [3, 4].

*Correspondence to: Department of Soil and Water Sciences, The Hebrew University of Jerusalem, P.O. Box 12, Rehovot 76100, Israel

The deformation of unconsolidated (uncemented) particulate material is nonlinear–its bulk stiffness varies with its deformation [5]. This nonlinearity is attributed to: (a) variation of the intergranular contact area with the deformation; (b) path-dependency of the intergranular force-displacement relation associated with frictional slip; and (c) variations in the contact network [6, 7]. Cementing the contacts constrains relative motion of the grains; hence, it is expected to reduce the nonlinearity of the bulk response relative to that of unconsolidated materials [8].

Indeed, a relatively linear response, with small variations in the slope of the stress-strain curve and in the macroscopic elastic moduli, is predicted by several micromechanical models [8, 9, 10, 11, 12]. In these models, cemented materials are represented by a network of particles connected by breakable springs, where the spring stiffness is either fixed [10, 11] or dependent upon the deformation [8, 9, 12]. In [8, 9], the elastic foundation model was used together with the contact theories of Hertz and Mindlin [13] to describe the deformation of the cement and the grains, respectively. In the "parallel-bond" model [12], the intergranular loads are evaluated by summing two components: (i) due to direct grain-grain contact, computed using Hertz and Mindlin models for uncemented grains, and (ii) loads exerted by cement deformation, represented by a linear-elastic beam. While the models in [8, 9] reproduce the variability of the macroscopic elastic moduli with porosity for loose samples [14], they predict minor changes in moduli for dense samples in which the porosity is only slightly modified with confining stress. Similarly, under stresses which are much lower than the sample's strength, the moduli evaluated in [12] remain nearly constant.

However, recent experiments reveal significant variations in the mechanical properties of weakly-consolidated sediments with their deformation, even under relatively small loads [15, 16, 3, 17]. Compressional and shear ultrasonic velocities measured along the axis of cylindrical samples were shown to increase with the applied uniaxial load, indicating stiffer response (Figure 1) [17]. Increasing the degree of cementation (reducing porosity) reduces the nonlinearity—only slight increase in stiffness with stress is observed in the well-cemented samples. In triaxial tests, stress-strain data during unloading-reloading cycles did not coincide with the main loading curve, and the Young's modulus increased with stress [3]. Finally, acoustic emissions soon after loading begins suggest early development of microcracks [15], which are associated with inelastic bulk deformation [18].

In this paper, we study the micromechanical origins for the nonlinear deformation of weakly-cemented sediments. We simulate loading of a three-dimensional (3-D), irregular packing of spherical grains. We model the physics at the grain-scale, accounting for intergranular mechanical interactions by performing all computations at the grain level. The collective behavior of the grains determines the bulk response of the grain pack. We demonstrate that the nonlinear deformation of cemented contacts, such as that emanating from opening/closure of microcracks, granular cement and sub-grain scale heterogeneity, governs the bulk response. A model in which the contact stiffness is an exponential function of the local deformation reproduces the experimental data well. We show that the assumption of linear-elastic cement deformation, where the main source of nonlinearity is the change in contact area described by Hertzian-type model, underestimates the rate of bulk stiffening with stress.

The paper is organized as follows. Section 2 describes our grain-scale model: outline (2.1), intergranular constitutive relations (2.2), and simulation methodology including the generation of a numerical packing (2.3) and the evaluation of equilibrium configurations (2.4) and macroscopic

parameters (2.5). The results are presented in Section 3. Section 3.1 lists the parameter values used in the simulations. In Sections 3.2 we compare our results with experimental data. Section 3.3 examines the impact of the intergranular constitutive rules and parameter values on the bulk response. Section 4 concludes this work.

2. MICROMECHANICAL MODEL OF WEAKLY-CEMENTED SEDIMENT

2.1. Quasi-Static Granular Model

We simulate the deformation of a cemented sample using Quasi-Static Granular Model (QuSGM) [6, 7, 19]. QuSGM is a mechanistic grain-scale model which accounts for intergranular interactions through constitutive rules derived from contact mechanics theories. In QuSGM, a computer-generated irregular 3-D pack of spherical grains is loaded by incremental displacement of its boundaries. Deformation is described by a sequence of static equilibrium configurations of the grains. A variational approach is employed to find these configurations by minimizing the total work against the intergranular loads. Macroscopic elastic moduli of the pack are evaluated from the intergranular forces and the boundary displacement. The implementation of QuSGM in modeling cemented sediments is described below.

2.2. Constitutive relations for cemented grains

We compute the intergranular loads from the grain displacements through a set of constitutive rules which are based on the following conceptual model: each pair of cemented grains is represented by an elastic beam which deforms due to relative displacement of its ends (grain centers), see Figure 2. The beam stiffness, an effective property of both the grain pair and the cement, changes with its deformation. Possible mechanisms that can lead to highly nonlinear deformation of a cemented contact include: (1) formation, closure, and reopening of microcracks [20, 21]; (2) geometrical

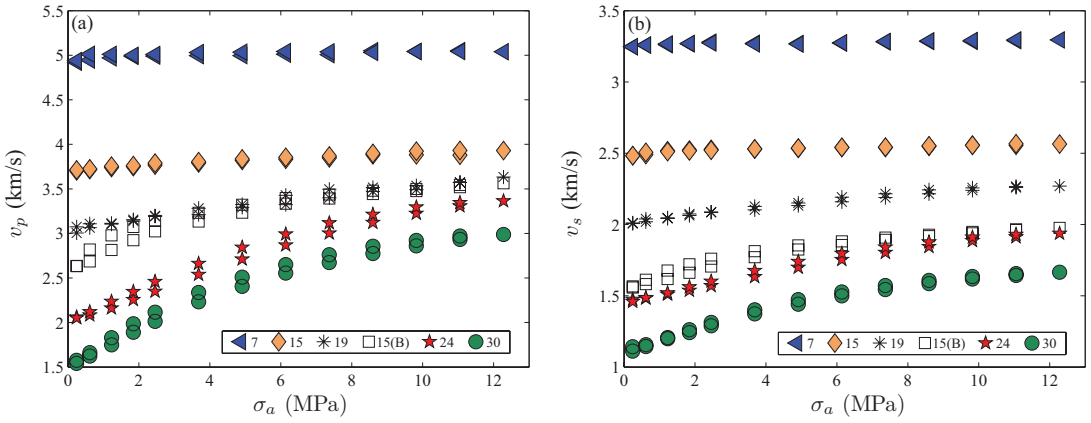

Figure 1. Increase in bulk stiffness with axial stress, σ_a, as indicated from the increase in compressional (a) and shear (b) ultrasonic velocities, v_p and v_s. The velocities were measured by [17] along the axis of cylindrical samples during uniaxial loading-unloading cycle (higher velocities during unloading) in synthetic samples of quartz grains cemented by soda-lime glass. The legend entries denote the sample porosity ϕ (%) achieved by introducing different amounts of cement (reducing the porosity from an initial value of 35%). Also shown are data for Berea sandstone ($\phi\approx$15%, square symbols).

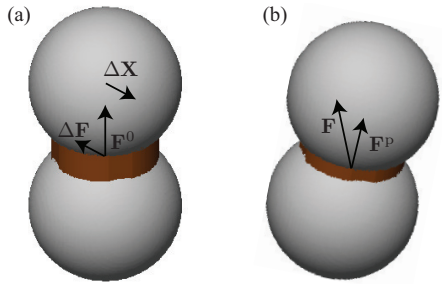

Figure 2. Conceptual model of a pair of grains cemented at their contact. We compute the intergranular load in analogy with an elastic beam, which deforms due to relative displacement of its ends (grain centers). The load acting on the top grain at a given reference configuration (a), $\mathbf{F}^0$, is perturbed due to a relative displacement of $\Delta\mathbf{X}$. The load at the current configuration (b), $\mathbf{F}$, is updated by adding a load increment, $\Delta\mathbf{F} = -k^*\Delta\mathbf{X}$, to a projection of $\mathbf{F}^0$ (accounting for the rotation of the contact area), $\mathbf{F}^p$. The parameter k^* represents the effective (composite) stiffness of the cemented grain pair.

nonlinearities due to granular cement (e.g. see Figures 2–5 in [22]); and (3) material heterogeneity. One example of the effect of material heterogeneity is a grain pair cemented by a softer material. Under a small load the deformation is localized close to the contact interface [13], within the softer cement. With further compression, the deformation extends into the stiffer grain material, and the effective contact stiffness increases.

The contact mechanics theories of Hertz, Mindlin and Deresiewicz [13, 23, 24] evaluate the contact stiffness for uncemented particles. To obtain an effective stiffness that includes the effect of cement, we use a model based on those in [23, 24], however with: (a) effective (cemented) contact area; (b) restricted intergranular sliding; and (c) cohesive (tensile) forces. We model the effect of mechanisms such as microcracks, geometrical nonlinearities and material heterogeneities through a strong dependence of the effective stiffness on the contact deformation.

We focus on early stages of loading, with stresses much smaller than the yield stress. Hence, our model does not account for complete failure (fracturing) of either grains or cement, a simplification justified by the following two observations. First, experiments with natural and synthetic sediments suggest that fracturing of mineral grains occurs under very high stresses, and that the cement material, usually weaker than the grains, yields first [1, 25, 15]. Secondly, while stress concentration may fracture the cement even at low stresses, numerical simulations show that the bulk response at that stage is mainly controlled by the behavior of the intact, cemented contacts [15].

The resulting force-displacement relations are used to update the intergranular forces as they vary with the macroscopic load, applied by a sequence of incremental boundary displacements. The current configuration serves as the reference configuration of the next step. At each (load) step, the (current) load acting on a grain, $\mathbf{F}$, is evaluated by $\mathbf{F} = \mathbf{F}^p + \Delta\mathbf{F}$. Here, $\mathbf{F}^p$ is the projection of the intergranular load at the reference configuration ($\mathbf{F}^0$), accounting for the rotation of the contact area (Figure 2). The force increment $\Delta\mathbf{F} = -k^*\Delta\mathbf{X}$ is proportional to the incremental (measured with respect to the reference configuration) relative displacement between the grains, $\Delta\mathbf{X}$. The effective stiffness k^* is evaluated at the reference configuration. Superscript * denotes an effective contact property. In the following Sections, the force-displacement relations for normal, shear and torsional components are formulated.

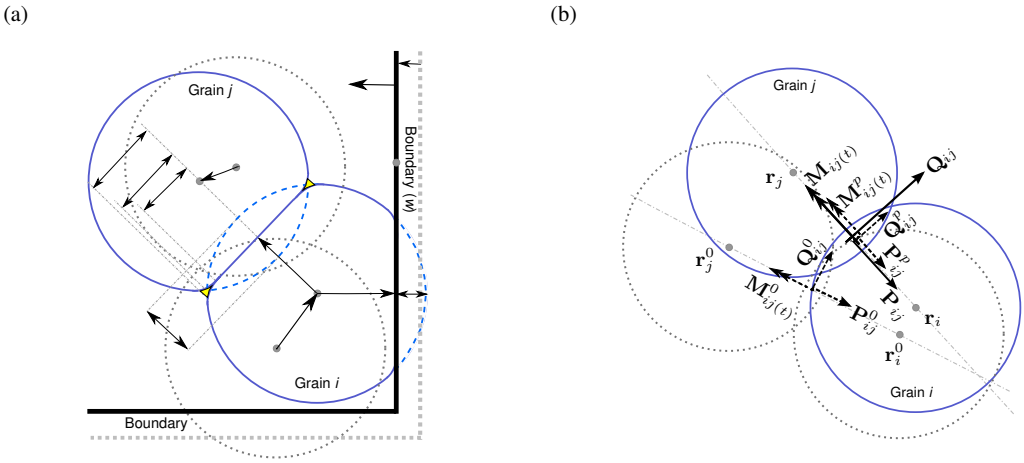

Figure 3. Schematic of the grain-scale model: (a) Contact geometry. The reference configuration of the grains and boundaries is marked with grey dotted lines. Dashed lines denote the shape of undeformed grains in the current configuration, following an incremental displacement of the sample boundaries. (b) The loads on grain i at a cemented contact with grain j at the reference (superscript 0) and current configuration, plotted as dashed and solid arrows, respectively. The current loads are computed by adding a load increment to a projection of the reference loads onto the current contact area to account for its rotation (superscript p).

2.2.1. Normal component of the intergranular force In analogy with Hertz contact model [13], we assume that the intergranular normal force is unaffected by shear and torsion and can be computed independently. Let us consider a pair of cemented grains, i and j. We use a single index, $1, 2, \ldots, N$, to label each grain, where N is the number of grains in the pack. At a given (reference) configuration, the deformation of the cement and grain material imposes a normal force $\mathbf{P}^0_{ij}$ on grain i. Due to the cohesion introduced by cement, this force can be either compressive or tensile. Following an incremental boundary displacement, the normal force becomes

$$\mathbf{P}_{ij} = \mathbf{P}^p_{ij} - k^*_{ij(n)}\mathbf{u}_{ij(n)}, \tag{1}$$

where $k^*_{ij(n)}$ is the effective normal stiffness of the contact, that is its resistance to compression/tension. Hereafter, we use subscripts $_{(n)}$, $_{(s)}$, and $_{(t)}$ to denote the normal, shear and torsional components, respectively. The term $\mathbf{P}^p_{ij} = \left\|\mathbf{P}^0_{ij}\right\| \operatorname{sgn}\left(\mathbf{P}^0_{ij}\cdot\hat{\mathbf{r}}_{ij}\right)\hat{\mathbf{r}}_{ij}$ accounts for the effect of the contact interface reorientation on the force direction, where $\hat{\mathbf{r}}_{ij} = \mathbf{r}_{ij}/\|\mathbf{r}_{ij}\|$. The radius vector $\mathbf{r}_{ij} = \mathbf{r}_i - \mathbf{r}_j$ connects the centers of grain i and j (Figure 3). The rectangular sample is bounded by planar elastic walls. For a contact with a planar boundary w ($w = 1, 2, \ldots, 6$), $\hat{\mathbf{r}}_{ij}$ in the above expression is replaced with the outward normal to that boundary, $\hat{\mathbf{n}}_w$. The normal component of the incremental displacement of grain i relative to another grain j or a boundary w is

$$\mathbf{u}_{ij(n)} = \hat{\mathbf{r}}_{ij}\otimes\hat{\mathbf{r}}_{ij}\left(\mathbf{u}_i - \mathbf{u}_j\right) \qquad \text{for a grain-grain contact} \tag{2a}$$

$$\mathbf{u}_{iw(n)} = \hat{\mathbf{n}}_w\otimes\hat{\mathbf{n}}_w\left(\mathbf{u}_i - \mathbf{u}_w\right) \qquad \text{for a grain-boundary contact.} \tag{2b}$$

Here $\mathbf{u}_i = \mathbf{r}_i - \mathbf{r}^0_i$ and $\mathbf{u}_w = \mathbf{x}_w - \mathbf{x}^0_w$ are the displacements of a grain and a boundary relative to the previous (load) step, $\mathbf{x}_w$ is an arbitrary point on the boundary, and $\otimes$ is the tensor product.

For each load step, the normal stiffness $k^*_{ij(n)}$ is evaluated from the contact deformation in the following manner. We begin with the expression for the compressive force in Hertz theory,

$P_{ij} = (4/3)E_{ij}R_{ij}^{1/2}h_{ij}^{3/2}$, where $R_{ij} = (1/R_i + 1/R_j)^{-1}$, $E_{ij} = \left[(1-\nu_i^2)/E_i + (1-\nu_j^2)/E_j\right]^{-1}$, and R_i, E_i and ν_i denote the radius, Young's modulus and Poisson's ratio of grain i [13]. The intergranular deformation is parameterized by the mutual approach, $h_{ij} = R_i + R_j - \|\mathbf{r}_{ij}\|$. For a contact with a planar boundary w, $h_{iw} = R_i - (\mathbf{r}_i - \mathbf{x}_w)\cdot\hat{\mathbf{n}}_w$. Next, we perform a Taylor series expansion of P_{ij} near h_{ij}^0. Assuming the change in h_{ij} is only due to the normal displacement increment, we obtain $dh_{ij} \sim \|\mathbf{u}_{ij(n)}\|$. Finally, with the definition for the contact radius in Hertz theory, $a_{ij} = (R_{ij}h_{ij})^{1/2}$, approximating the force increment by the first-order term in the expansion, $k_{ij(n)}^*\|\mathbf{u}_{ij(n)}\| \sim 2E_{ij}\ a_{ij}^*\big|_{h_{ij}^0}\ dh_{ij}$, provides

$$k_{ij(n)}^* = 2E_{ij}a_{ij}^*. \tag{3}$$

In obtaining $k_{ij(n)}^*$ (as well as the shear and torsional stiffness) we use an effective contact radius, a_{ij}^*. Its evaluation is explained in Section 2.2.4. Since we consider only small amounts of intergranular cement, we compute the effective stiffness (for normal, shear and torsion) using the moduli of the grain material (E_i, ν_i) rather than a combination of the grain and the cement moduli.

2.2.2. Tangential component of the intergranular force Consider a pair of cemented grains, where the tangential force component applied on grain i due to its contact with grain j is $\mathbf{Q}_{ij}^0$. A relative tangential displacement $\mathbf{u}_{ij(s)}$ alters the tangential force, which is updated by

$$\mathbf{Q}_{ij} = \mathbf{Q}_{ij}^p - k_{ij(s)}^*\mathbf{u}_{ij(s)}, \tag{4}$$

where $k_{ij(s)}^*$ is the effective shear stiffness. The reorientation of the contact area is modeled by $\mathbf{Q}_{ij}^p = \left\|\mathbf{Q}_{ij}^0\right\|\hat{\mathbf{t}}_{ij}$, where $\hat{\mathbf{t}}_{ij} = \mathbf{T}_{ij}\mathbf{Q}_{ij}^0/\left\|\mathbf{T}_{ij}\mathbf{Q}_{ij}^0\right\|$ and $\mathbf{T}_{ij} = \hat{\mathbf{I}} - \hat{\mathbf{r}}_{ij}\otimes\hat{\mathbf{r}}_{ij}$. For a contact with a boundary w, $\mathbf{T}_{iw} = \hat{\mathbf{I}} - \hat{\mathbf{n}}_w\otimes\hat{\mathbf{n}}_w$. The relative tangential displacement of grain i with respect to grain j or boundary w is

$$\mathbf{u}_{ij(s)} = \mathbf{T}_{ij}(\mathbf{u}_i - \mathbf{u}_j) + \boldsymbol{\Omega}_i\times\mathbf{R}_{ij} - \boldsymbol{\Omega}_j\times\mathbf{R}_{ji} \tag{5a}$$

$$\mathbf{u}_{iw(s)} = \mathbf{T}_{iw}(\mathbf{u}_i - \mathbf{u}_w) + \boldsymbol{\Omega}_i\times\mathbf{R}_{iw}, \tag{5b}$$

where $\boldsymbol{\Omega}_i$ denotes the incremental rotation (relative to the reference configuration) of grain i by an angle $\|\boldsymbol{\Omega}_i\|$ around an axis passing through its center and directed along $\boldsymbol{\Omega}_i$. Here, $\mathbf{R}_{ij} = -\hat{\mathbf{r}}_{ij}\sqrt{R_i^2 - A_{ij}^2}$ and $\mathbf{R}_{iw} = -\hat{\mathbf{n}}_w\,(R_i - h_{iw})$ are radius-vectors connecting the center of grain i to the center of the contact area with another grain j or boundary w, respectively, and $\times$ denotes the vector product (using the right-hand convention). The intersection of the undeformed grain surfaces defines a disk of radius $A_{ij} = \sqrt{\left(R_{ij}^- - r_{ij}\right)\left(-R_{ij}^- - r_{ij}\right)\left(R_{ij}^+ - r_{ij}\right)\left(R_{ij}^+ + r_{ij}\right)}/(2r_{ij})$, where $R_{ij}^- = R_i - R_j$, $R_{ij}^+ = R_i + R_j$ and $r_{ij} = \|\mathbf{r}_{ij}\|$ (Figure 3).

The evaluation of the shear stiffness $k_{ij(s)}^*$ is based on the model in [23]. In [23], intergranular slip is modeled through a dependence of the stiffness on the loading history. The stiffness attains a maximum ("no-slip") value, $k_{ij(s)}^{\max} = 8a_{ij}/\left[(2-\nu_i)/G_i + (2-\nu_j)/G_j\right]$, at the onset of either loading or unloading (as the tangential force either increases from zero or decreases after monotonic loading), and vanishes at sliding ("complete slip"). Here, G_i is the shear modulus of the grain. While intact cement prohibits sliding between the grains, we argue that partial slip within granular cement,

along microcracks, or at the grain-cement interface, is an important deformation mechanism. Therefore, we evaluate the stiffness from the expression for $k_{ij(s)}^{\max}$ by: (1) substituting a_{ij}^* for a_{ij}; and (2) reducing its value by $C_s \leq 1$ to account for slip:

$$k_{ij(s)}^* = C_s 8 a_{ij}^* \left(\frac{2-\nu_i}{G_i} + \frac{2-\nu_j}{G_j} \right)^{-1}. \tag{6}$$

Following [23], the shear stiffness in our model depends on the normal deformation through the contact radius, a_{ij}^*. For simplicity, we do not account for the effect of the loading history and use a fixed C_s value to evaluate $k_{ij(s)}^*$.

2.2.3. Intergranular torque The torsional couple acting on a pair of cemented grains is evaluated by adapting the constitutive rule in [24], in a manner similar to that in Section 2.2.2. A pair of grains, i and j, is loaded by a torsional couple, with torque $\mathbf{M}_{ij(t)}^0$ applied on grain i. Following relative torsion between the grains, $\mathbf{\Omega}_{ij(t)}$, the torque becomes

$$\mathbf{M}_{ij(t)} = \mathbf{M}_{ij(t)}^p - k_{ij(t)}^* \mathbf{\Omega}_{ij(t)}, \tag{7}$$

where $\mathbf{M}_{ij(t)}^p = \left\| \mathbf{M}_{ij(t)}^0 \right\| \operatorname{sgn}\left(\mathbf{M}_{ij(t)}^0 \cdot \hat{\mathbf{r}}_{ij} \right) \hat{\mathbf{r}}_{ij}$ accounts for the rotation of the contact area (Figure 3). For a contact with a boundary w, $\mathbf{M}_{iw(t)}^p = \left\| \mathbf{M}_{iw(t)}^0 \right\| \operatorname{sgn}\left(\mathbf{M}_{iw(t)}^0 \cdot \hat{\mathbf{n}}_w \right) \hat{\mathbf{n}}_w$. The incremental torsion of grain i relative to grain j and boundary w is evaluated by

$$\mathbf{\Omega}_{ij(t)} = \left[(\mathbf{\Omega}_i - \mathbf{\Omega}_j) \cdot \hat{\mathbf{r}}_{ij} \right] \hat{\mathbf{r}}_{ij} \tag{8a}$$

$$\mathbf{\Omega}_{iw(t)} = (\mathbf{\Omega}_i \cdot \hat{\mathbf{n}}_w) \, \hat{\mathbf{n}}_w. \tag{8b}$$

We compute the torsional stiffness $k_{ij(t)}^*$ by reducing the no-slip value in [24] by a factor C_s and using the effective radius a_{ij}^*,

$$k_{ij(t)}^* = C_s \frac{16}{3} \left(a_{ij}^* \right)^3 \left[\frac{1}{G_i} + \frac{1}{G_j} \right]^{-1}. \tag{9}$$

The total moment applied on grain i relative to its center is evaluated from the sum of the torsional and shear components, $\mathbf{M}_{ij} = \mathbf{M}_{ij(t)} + \mathbf{M}_{ij(s)}$, where $\mathbf{M}_{ij(s)} = \mathbf{R}_{ij} \times \mathbf{Q}_{ij}$. We note that the small effect of intergranular torsion on the macroscopic stress [7] makes the macroscopic elastic moduli relatively insensitive to the exact value of $k_{ij(t)}^*$ (and C_s).

2.2.4. Evolution of the effective contact stiffness In our model, the dependence of the effective contact stiffness on the loading is through the effective contact radius, a_{ij}^*. Simulations begin with an initial, undeformed configuration, with an effective radius of

$$a_{ij}^{*,I} = (1+\kappa) \, a_{ij}^I, \tag{10}$$

where $a_{ij}^I = \left(R_{ij} h_{ij}^I \right)^{1/2}$. Superscript ^{I} denotes the initial state. A scalar parameter, κ, quantifies the effect of cement on the initial stiffness. For a given cement material and geometry, κ is a (nonlinear)

function of the cement content: higher κ corresponds to a higher degree of cementation. In the limit of negligible amount of cement, $\kappa \to 0$ and $a^*_{ij} \approx a_{ij}$.

To study the impact of cement deformation on the bulk response, we compare simulations with two types of stiffness evolution models: (a) linear-elastic cement, where the cement contribution to the contact stiffness remains fixed and the stiffness varies only due to the deformation of the grain material (as in Hertz model); and (b) nonlinear cement deformation, with a stronger dependence of the effective stiffness on the contact deformation.

Linear-elastic cement model To examine if changes in the grain-grain contact area govern the deformation process, we formulate a "linear-elastic cement" model in which the nonlinearity of the force-displacement relation is due to the change in normal compression of the grains alone. We assume that cement does not restrict the expansion of the grain-grain contact area, which is computed using Hertz model, $a_{ij} = (R_{ij}h_{ij})^{1/2}$. With that, the effective contact radius is

$$a^*_{ij} = (R_{ij}h_{ij})^{1/2} + \kappa a^I_{ij}. \tag{11}$$

If grains detach ($h_{ij} \leq 0$), a cohesive force is evaluated using $h_{ij} = 0$ in Eq. (11).

Nonlinear cement deformation To model grain-scale mechanisms such as opening and closure of microcracks, geometrical nonlinearity and material heterogeneity, we vary the effective contact stiffness with the deformation at a faster rate than in Eq. (11). In analogy with Hertz theory, we parametrize the contact deformation using a single strain-like parameter. We define a contact strain, $r^*_{ij} = \left(r^I_{ij} - r_{ij}\right)/r^I_{ij}$ (equivalent to the change in h_{ij} normalized by the initial intergranular distance), and assume the effective contact radius is an exponential function of this strain,

$$a^*_{ij} = a^{*,I}_{ij} \exp\left(\gamma r^*_{ij}\right). \tag{12}$$

The effective stiffness increases as grains become closer ($r^*_{ij} > 0$), and vice versa. The parameter γ corresponds to the rate of strain hardening of the contact under compression, and softening in tension. A physical justification for the selection of an exponential function is provided in Appendix A.

2.3. Initial configuration

The initial grain pack (grain positions and sizes) is generated numerically. The procedure begins with a loose irregular arrangement of spheres, here produced by a random generator. Then, the packing density is increased by a combination of (a) boundary displacements that mimic isotropic compaction; and (b) particle expansion, increasing the radius of spheres with low coordination number (less than 4 contacts) [6, 19]. Cement is represented through the initial effective contact radius $a^{*,I}_{ij}$ [Eq. (10)], where we assign a uniform κ for all contacts. To create a well-connected assembly of grains, we add cement at the contact of all grain pairs in close proximity, $h^I_{ij} \geq h^{\min}_{ij}$. Here, $h^{\min}_{ij} = -\varepsilon\left(R_i + R_j\right)$ and we use $\varepsilon = 0.1$. For a grain i adjacent to but not in contact with grain j ($0 \geq h^I_{ij} \geq h^{\min}_{ij}$), we compute $a^{*,I}_{ij}$ by replacing h^I_{ij} with the lowest positive h^I_{ij} value among

all contacting grains (j). This replacement is only performed in the exponential model [Eq. (12)]; therefore, the initial sample stiffness is lower for the linear-elastic cement model [Eq. (11)].

Following [12, 26, 4] we reduce the dependence of the results on the sample generation procedure by assuming a stress-free initial configuration, and measure the intergranular deformations and loads relative to that configuration.

2.4. Equilibrium configurations

Mechanical equilibrium is described by a system of force and moment balance equations,

$$\mathbf{F}_i = \sum_{j=1}^{N_g^i} (\mathbf{P}_{ij} + \mathbf{Q}_{ij}) + \sum_{w=1}^{N_b^i} (\mathbf{P}_{iw} + \mathbf{Q}_{iw}) - m_i g \hat{\mathbf{e}}_z = \mathbf{0} \tag{13a}$$

$$\mathbf{M}_i = \sum_{j=1}^{N_g^i} \left(\mathbf{M}_{ij(s)} + \mathbf{M}_{ij(t)}\right) + \sum_{w=1}^{N_b^i} \left(\mathbf{M}_{iw(s)} + \mathbf{M}_{iw(t)}\right) = \mathbf{0}, \tag{13b}$$

where $\mathbf{F}_i$ and $\mathbf{M}_i$ are the sum of forces and moments acting on grain i, $\hat{\mathbf{e}}_z$ is a unit vector pointing opposite to the direction of gravity, g is the gravitational acceleration, and $m_i = (4/3)\pi R_i^3 \rho_i$ is the grain's mass, given its density ρ_i. The summation is done over the number of contacts of grain i with other grains (N_g^i) and boundaries (N_b^i), where $N_g^i + N_b^i$ is its coordination number.

In QuSGM, the equilibrium configurations are evaluated using the principle of least work [27]. For a given reference configuration, we seek a (local) minimum of the total work Π done against the loads acting on the grains following a perturbation of the boundaries, with respect to the generalized coordinates, $\boldsymbol{\theta} = [\mathbf{u}_1 \ldots \mathbf{u}_N \quad \boldsymbol{\Omega}_1 R_1 \ldots \boldsymbol{\Omega}_N R_N]$. The value of $\boldsymbol{\theta}$ that corresponds to the minimum of Π provides the next equilibrium configuration. The functional Π is computed by

$$\Pi(\boldsymbol{\theta}) = -\sum_{i=1}^{N} \left\{ \frac{1}{2} \sum_{j=1}^{N_g^i} W_{ij} + \sum_{w=1}^{N_w^i} W_{iw} - m_i g (\mathbf{u}_i \cdot \hat{\mathbf{e}}_z) \right\}, \tag{14}$$

where $W_{ij} = W_{ij(n)} + W_{ij(s)} + W_{ij(t)}$ is the total work done against the normal, tangential and torsional loads acting on a grain pair ij, evaluated by integrating the product of the loads and the generalized coordinates. The integration is performed numerically using a midpoint rectangular rule,

$$W_{ij(n)} = \mathbf{P}_{ij}^p \cdot \mathbf{u}_{ij(n)} - \frac{1}{2} k_{ij(n)}^* \left\|\mathbf{u}_{ij(n)}\right\|^2 \tag{15a}$$

$$W_{ij(s)} = \mathbf{Q}_{ij}^p \cdot \mathbf{u}_{ij(s)} - \frac{1}{2} k_{ij(s)}^* \left\|\mathbf{u}_{ij(s)}\right\|^2 \tag{15b}$$

$$W_{ij(t)} = \mathbf{M}_{ij(t)}^p \cdot \boldsymbol{\Omega}_{ij(t)} - \frac{1}{2} k_{ij(t)}^* \left\|\boldsymbol{\Omega}_{ij(t)}\right\|^2. \tag{15c}$$

We use a conjugate gradient algorithm to find the minimum of Π, see [7, 19]. When Π is at a minimum, its gradient with respect to $\boldsymbol{\theta}$, $\nabla_{\boldsymbol{\theta}}\Pi = -[\mathbf{F}_1 \ldots \mathbf{F}_N \quad \mathbf{M}_1/R_1 \ldots \mathbf{M}_N/R_N]$, vanishes. Thus, the equality of the gradient to zero corresponds to the equilibrium configuration. Computing k^* at the reference configuration makes the system of equations [Eq. (13)] piece-wise linear.

2.5. Macroscopic parameters

At each load step, we evaluate the macroscopic strain $\boldsymbol{\epsilon}$, stress $\boldsymbol{\sigma}$ and elastic moduli of the sample. The strain, applied by normal displacements of the planar sample boundaries, is evaluated by normalizing these displacements by the initial (undeformed) sample size. The normal stresses are computed by summing the intergranular normal forces applied on the boundary walls and dividing by the walls' area. The elastic moduli at a given stress state are found by fitting a stress-strain interval centered around that state with Hooke's law for a homogeneous, isotropic material [7, 19].

3. RESULTS

3.1. Simulation parameters

We simulate experiments in which a pack of cemented round quartz grains is loaded uniaxially [3, 17]. To mimic uniaxial loading we maintain negligible lateral macroscopic stresses by applying compressive axial strain increments $\Delta\epsilon_a$ together with tensile lateral strain increments $\Delta\epsilon_l = \nu_{\text{mac}}\Delta\epsilon_a$, using Poisson's expansion of $\nu_{\text{mac}} = 0.25$. The initial dense sphere packing was generated by simulating isotropic compression of a loose arrangement (with confinement of 10 MPa, see [19]). Then, we install a uniform cement content ($\kappa = 1\%$ in all simulations, unless noted otherwise), and measure the macroscopic stress and strain relative to that configuration. We represent quartz sand by assigning the following values to the grains: (a) density of $\rho_i = 2.65\,\text{gr/cm}^3$; (b) uniform radii distribution, $R_i \in [0.07, 0.13]$ mm; and (c) elastic moduli from a normal distribution with mean values of $\bar{E} = 100\,\text{GPa}$ for Young's modulus, $\bar{\nu} = 0.15$ for Poisson's ratio, and a standard deviation of 0.1 [19]. Intergranular slip is represented by $C_s = 1/10$ [Eq. (6)].

3.2. Reproduction of experimental data

We compare our results with the experimental data in [3, 17]. In [3], a sample of quartz grains bonded by Portland cement (0.29 weight fraction of total sample, porosity of $\phi \approx 22\%$) was loaded uniaxially, with intermittent unloading-reloading cycles at different stresses. The macroscopic Young's modulus, E, was estimated from the unloading curves. The stiffness E for the sample with $\phi \approx 30\%$ in Figure 1 [17] (quartz grains cemented by soda-lime glass) is evaluated from the acoustic velocities assuming a planar wave in an infinite, isotropic medium [5]. The rapid moduli increase with stress observed in the experiments is reproduced in simulations with the exponential stiffness evolution model (Figure 4).

Since we study the deformation during initial loading, we do not extend our simulations beyond stress of $\sim$5 MPa. Under larger stress, closer to the sample's strength, deformation mechanisms such as coalescence of microcracks may become important [18, 21, 28, 16, 15, 3]. These mechanisms reduce the rate of stiffening as the macroscopic stress approaches the strength (pre-failure), and cause softening of the sample once it has failed (see inset in Figure 4). The effect of these mechanisms is not accounted for in our model, which therefore cannot predict the observed pre- and post-failure behavior.

Finally, while both experiments [3, 17] show similar stiffening behavior under low stresses, their setup and the samples tested are different, and, therefore, comparison of the evaluated moduli is

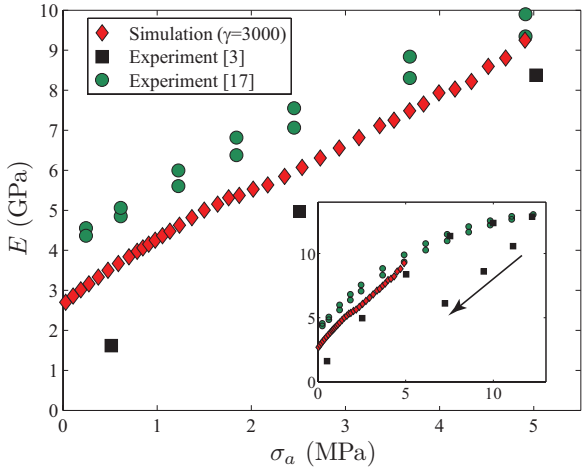

Figure 4. Evolution of the macroscopic stiffness (Young's modulus E) with axial stress (σ_a), obtained from: (1) our simulations of uniaxial loading using the exponential stiffness evolution model with $\gamma = 3000$; (2) uniaxial loading-unloading experiment with sand grains bonded by Portland cement (data obtained by digitizing Figure 2(b) in [3]); and (3) acoustic testing of a pack of quartz grains cemented by soda-lime glass, during an axial loading-unloading cycle (higher stiffness during unloading) [17]. The rapid stiffness increase with loading is reproduced by the exponential model. We focus on the initial loading stage and thus do not simulate loading above $\sim$5 MPa. Further loading leads to a decrease in the stiffening rate prior to macroscopic failure, and post-failure softening (see arrow in inset). This behavior is associated with coalescence of microcracks and possibly other mechanisms, which are not accounted for in our model.

sensible only under limited range of conditions. One difference is the type of loading—static [3] vs. dynamic [17]. However, the difference between static and dynamic moduli is small if the wavelength is sufficiently larger than the individual grain size [9, 5], which is the case in the experiments by [17] (by a factor of $\sim$10), and if the static moduli are evaluated from small-amplitude unloading cycles during loading (therefore minimizing the effect of stress-induced anisotropy [29]), as performed in [3]. In addition, the two samples have different cement material, cement content, and porosity, and therefore their deformation may be governed by different mechanisms: geometrical nonlinearity associated with granular and relatively soft cement is likely to be dominant in [3], whereas microcracks within the stiff soda-lime glass can strongly affect the bulk response in [17]. Frictional sliding along microcracks is inhibited in well-cemented materials (low porosity samples in Figure 1), hence limiting the increase in bulk stiffness with stress.

3.3. Micromechanical impact on the bulk stiffness

The macroscopic elastic moduli of the sample in our model are computed from the intergranular loads. Hence, the bulk stiffness evolution reflects the collective mechanical interactions at the grain-scale. Below, we investigate the impact of the intergranular constitutive rules and the grain-scale parameters introduced here (γ, C_s and κ) on the bulk stiffness.

3.3.1. Intergranular constitutive rules Here, we examine the effect of the intergranular constitutive relations on the bulk response by comparing simulations with different stiffness evolution models: (1) exponential model [Eq. (12)] with $\gamma = 3000$; (2) exponential model, $\gamma = 1000$; (3) linear-elastic intergranular deformation with fixed effective stiffness, $\gamma = 0$; and (4) linear-elastic cement model [Eq. (11)]. We show that only the exponential model yields a stress-strain curve with appreciable

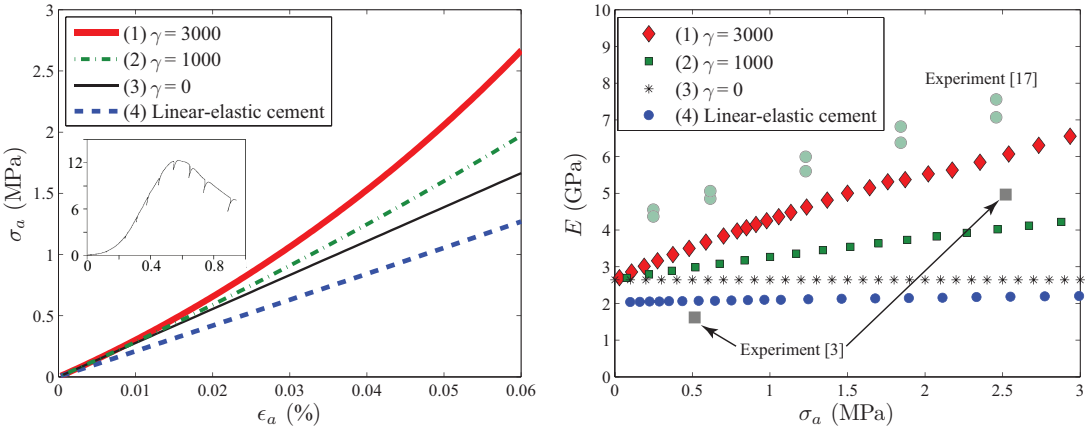

Figure 5. Impact of the intergranular constitutive relations on the macroscopic response, demonstrating the strong nonlinearity of the grain-scale deformation. Data from simulations using: (1) exponential model [Eq. (12)] with $\gamma = 3000$; (2) exponential model, $\gamma = 1000$; (3) linear-elastic intergranular deformation with fixed effective stiffness, $\gamma = 0$; and (4) linear-elastic cement model [Eq. (11)]. Only the exponential model, in which the intergranular stiffness rapidly changes with the local deformation, provides an appreciable convexity of the axial stress-strain curve (a, inset shows experimental data from Figure 2(a) in [3]) and significant stiffening with stress (b). In particular, a high exponent value, $\gamma = 3000$, is required to match the experimentally-evaluated moduli (semi-transparent disks [17] and squares [3]). Assuming linear-elastic cement with fixed contact stiffness (3) or with Hertzian intergranular interactions (4) underestimates the stiffness increase with stress.

convexity and rapid stiffening with the deformation. Moreover, a high exponent value (γ=3000) is required to match the experimental data[†]; using a lower exponent value underestimates the rate of moduli increase with stress (Figure 5). The exponent represents the change in the stiffness of a cemented contact with the deformation, for instance due to microcracks (Appendix A). Accurate prediction of the bulk stiffness from grain-scale parameters requires a rigorous evaluation of γ (as well as other micromechanical parameters we introduce here, C_s and κ) through sub-grain scale, mechanistic modeling of microcracks and heterogeneities. Since the main purpose of this work is to highlight the importance of grain-scale nonlinearity rather than gaining predictive capabilities, the values of these parameters that best fit the data were found by trial and error. Therefore, these values may not be representative of samples with different grain or cement material, cement quantity, or microstructure. Nonetheless, the good agreement between the exponential model with a large exponent value and the experiments demonstrates the highly-nonlinear nature of the intergranular deformation.

Conversely, models based on the hypothesis of linearly-elastic cement deformation (3–4 in Figure 5) and hence contact stiffness which varies only slightly (or not at all, in 3) with the deformation, predict a relatively linear bulk response, with nearly constant moduli. The nearly-constant stiffness evaluated by model 3 highlights the minor effect of changes in the coordination number (caused by grain rearrangements) in a cemented sample. Mild moduli variations, regardless of the choice of model parameters, were also evaluated by a parallel-bond type model (assuming nonlinear grain deformation and linear-elastic cement) [19]. The stiffness evaluated by model 4 is

[†]The absolute stress-strain values in our simulations are significantly lower that the experimental values [Figure 5(a)], due to our assumption of stress-free initial configuration, where the loads and deformations are measured relative to that configuration, see Section 2.3.

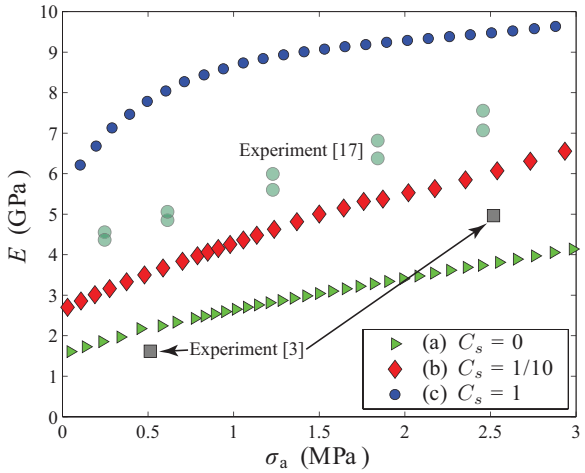

Figure 6. The effect of the shear stiffness reduction factor C_s, representing intergranular slip, on the bulk stiffness. We compare simulations using the exponential model with $\gamma = 3000$, assuming: (a) complete slip (sliding), $C_s = 0$; (b) partial slip, $C_s = 1/10$ (similar to Figure 4); and (c) no-slip, $C_s = 1$. The assumption of complete slip leads to an underestimation of the rate of stiffness increase with stress, whereas assuming no-slip overestimates the bulk stiffening. Using an intermediate value ($C_s = 1/10$) to account for partial slip provides good agreement with experimental data (superimposed as semi-transparent disks [17] and squares [3]), implying that slip is an important mechanism of considerable impact on the bulk stiffness.

significantly lower than in models 1–3 because of the small stiffness of cemented contacts with no direct grain-grain contact ($h_{ij} < 0$) in that model, computed with $a^*_{ij} = \kappa a^I_{ij}$. The inability of the models assuming linear-elastic cement and Hertzian grain-grain interaction to reproduce the experimental data demonstrates the highly-nonlinear deformation of cemented contacts, a nonlinearity which cannot be explained by Hertz model. A similar conclusion was drawn in [3].

3.3.2. Intergranular slip We represent the effect of slip on the intergranular shear stiffness by a reduction factor C_s [Eq. (6)]. We study the role of slip by comparing the bulk stiffness E obtained from simulations using the exponential model (γ=3000), assuming: (a) complete slip (sliding), C_s=0 ($k^*_{ij(s)}$=0); (b) partial slip, C_s=1/10; and (c) no-slip, C_s=1. As expected, larger C_s provides both higher initial bulk stiffness and stiffening rate. Assuming complete slip underestimates the rate of moduli increase with stress, whereas the no-slip assumption leads to its overestimation (Figure 6), regardless of the value of γ. An intermediate value of C_s=1/10 was found to best fit the experimental data (Figure 4). These results suggest that partial slip, for example at the grain-cement interface or within the cement, is a crucial mechanism that strongly affects the bulk response of weakly-cemented materials.

3.3.3. Cement content The initial (undeformed) effective contact radius and stiffness depend upon the parameter κ [Eq. (10)]. For small amounts of a given cement material deposited preferentially around the grain contacts, κ corresponds to the cement quantity (uniformly assigned to all contacts). To investigate the effect of κ on the evolution of the bulk stiffness with the deformation, we compare simulations using the exponential model ($\gamma = 3000$), for samples with $\kappa = 0.01$ (a, similar to Figure 4) and $\kappa = 0.2$ (b). As expected, the initial bulk stiffness of sample (b) is $\sim$20% higher than in sample (a). As loading proceeds, the stiffness of the two samples becomes comparable, implying

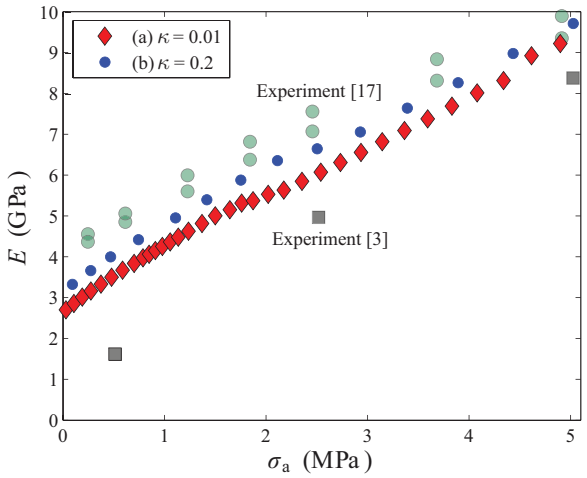

Figure 7. The impact of the cement content on the bulk stiffness, in simulations (exponential model, $\gamma = 3000$) using two samples with $\kappa = 0.01$ (a) and $\kappa = 0.2$ (b). The larger cement content in sample (b) provides an initially stiffer response. As loading proceeds, the stiffness of sample (a) increases faster than in (b), due to the reduced constraints imposed on grain rearrangements by the smaller cement content. Experimental data is superimposed (semi-transparent disks [17] and squares [3]).

faster stiffening with stress in (a) [Figure 7]. The faster hardening in sample (a) can be explained by the reduced constraints imposed on grain rearrangements by the smaller cement content: the more compliant contacts in (a) allow larger rearrangements, hence faster increase in intergranular stiffness as well as in the coordination number. We note that the sensitivity of our model to the value of κ (selected to fit the experimental data in [17, 3]) is lower than to γ and C_s, therefore both simulations (a, b) are in relatively good agreement with the experiments.

A significant increase in sample stiffness was observed in experiments as a result of adding small amounts of cement at the grain contacts [1]. To demonstrate this effect, we compare the results for sample (a) with QuSGM simulations of triaxial test on uncemented samples [6, 7]. Using a frictionless contact model provides Young's modulus of 0–0.5 GPa for axial stresses of 0–24 MPa [6]. Higher moduli (1.6–2.3 GPa, for a stress range of 8–25 MPa) are predicted by a model which accounts for intergranular friction (with friction coefficient of 0.3) and slip [7]. The stiffer response (2.7–9.2 GPa for stress of 0–5 MPa) of sample (a) with low cement quantity ($\kappa = 0.01$) shows the effect of inhibition of grain rearrangements by the cement.

4. SUMMARY AND CONCLUSIONS

A significant increase in the stiffness of weakly-cemented sediments with loading has been observed experimentally, yet is not predicted by published micromechanical models. To examine the source of this discrepancy, we have simulated loading of a weakly-cemented granular sample using several micromechanical models. In particular, we represent highly-nonlinear grain-scale deformation mechanisms such as closure and opening of microcracks, granular cement and material heterogeneity, by introducing an effective contact stiffness which varies with the local deformation. Our model relies on contact mechanics theories, where we introduce three additional grain-scale parameters that account for the effect of the cement content, intergranular slip, and intergranular

strain-hardening. A rigorous evaluation of these parameter values requires a mechanistic sub-grain scale model. Here, because we seek to demonstrate the significance of grain-scale nonlinearity rather than providing a predictive model, we select these parameter values by fitting the bulk stiffness with experimental data. We describe the grain-scale physics by performing all computations at the grain level. The bulk response results from the collective behavior of the individual grains.

Our results indicate that the assumptions (common to many micromechanical models) that cement is linear-elastic and that the main source of nonlinearity is contact area variations due to grain deformation described by Hertz contact model, lead to underestimation of the bulk stiffening rate. Conversely, accounting for highly-nonlinear grain-scale deformation by an exponential dependence of the contact stiffness on the deformation, with a large exponent value, reproduces the experimental data. Finally, sensitivity analysis suggests that intergranular slip, either within the cement or at the grain-cement interface, is a crucial mechanism of considerable impact on the bulk response. Our findings highlight the importance of adequate account of grain-scale mechanisms in modeling poorly-consolidated sediments.

APPENDIX A: EXPONENTIAL EVOLUTION OF THE INTERGRANULAR STIFFNESS

This appendix provides a physical justification for the selection of an exponential function to describe the intergranular stiffness evolution of weakly-cemented contacts [Eq. (12)]. We hypothesize that the primary cause for the nonlinear deformation of cemented contacts is microcracks, either within the cement or at the grain-cement contact. We use scaling analysis to arrive from the experimentally-observed exponential relation between the fracture (crack) normal effective stress and the fracture aperture [30], to the exponential relation between the effective contact radius (stiffness) and the contact strain.

The fracture normal stiffness, $k_n = d\sigma_n/d\Delta a$, is defined as the change in effective normal stress σ_n with the increment of fracture aperture Δa. Experiments show that the fracture stiffness is proportional to the normal stress, $k_n = C\sigma_n$, where the proportionality constant $C = dk_n/d\sigma_n$ is referred to as the "stiffness characteristic" ([30] and the references therein). Combining these two expressions for k_n results with an exponential dependence of the stress and the aperture:

$$\sigma_n \sim \exp\left(C\Delta a\right). \tag{A1}$$

Our hypothesis regarding the contribution of microcracks to the intergranular nonlinear deformation suggests that the normal force and relative displacement at a contact scale with the effective normal stress and aperture of the fracture, $P_{ij} \sim \sigma_n$ and $\|\mathbf{u}_{ij(n)}\| \sim \Delta a$. Substituting these parameters into Eq. (A1) provides $P_{ij} \sim \exp\left(C'\|\mathbf{u}_{ij(n)}\|\right)$, where the constant C' scales with the stiffness characteristic, $C' \sim C$. Using Eq. (1) together with the definition of the effective contact stiffness, $k^*_{ij(n)} = dP_{ij}/d\|\mathbf{u}_{ij(n)}\|$, provides $k^*_{ij(n)} \sim C' \exp\left(C'\|\mathbf{u}_{ij(n)}\|\right)$. Using the relation $k^*_{ij(n)} = 2E_{ij}a^*_{ij}$ [Eq. (3)] we get

$$a^*_{ij} \sim C'' \exp\left(C'\|\mathbf{u}_{ij(n)}\|\right). \tag{A2}$$

Finally, substituting $\|\mathbf{u}_{ij(n)}\|$ in Eq. (A2) by the more general contact strain r^*_{ij} and normalizing by the initial state leads to Eq. (12), $a^*_{ij} = a^{*,I}_{ij} \exp\left(\gamma r^*_{ij}\right)$, with $\gamma \sim C'$. This simple scaling analysis explains our choice of an exponential function for the evolution of the effective contact stiffness. This analysis also suggests a physical interpretation for the exponent γ: it is related to the stiffness characteristic, $C = dk_n/d\sigma_n$, which describes the change in fracture (contact) stiffness with stress. The observation of a relatively constant value of C [30] supports our use of a constant γ value, that does not change with the deformation.

ACKNOWLEDGEMENT

I am grateful to D.B. Silin and T.W. Patzek for their significant contribution to this work. I thank S. Nakagawa and Y. Bernabè for providing me with experimental data and for fruitful discussions, and two anonymous reviewers for their constructive evaluation. This work was partially supported by the Department of Energy under grant #DE-FC26-05NT42664.

REFERENCES

1. Bernabè Y, Fryer DT, Hayes JA. The effect of cement on the strength of granular rocks. *Geophysical Research Letters* 1992; **19**(14):1511–1514.
2. Tada R, Siever R. Pressure solution during diagenesis. *Annual Review of Earth and Planetary Sciences* 1989; **17**(1):89–118, doi:10.1146/annurev.ea.17.050189.000513.
3. Saidi F, Bernabè Y, Reuschlè T. The mechanical behaviour of synthetic, poorly consolidated granular rock under uniaxial compression. *Tectonophysics* 2003; **370**(1–4):105–120, doi:10.1016/S0040-1951(03)00180-X.
4. Garcia X, Medina E. Acoustic response of cemented granular sedimentary rocks: molecular dynamics modeling. *Physical Review E* 2007; **75**(6):061308, doi:10.1103/PhysRevE.75.061308.
5. Makse HA, Gland N, Johnson DL, Schwartz L. Granular packings: nonlinear elasticity, sound propagation and collective relaxation dynamics. *Physical Review E* 2004; **70**:061 302, doi:10.1103/PhysRevE.70.061302.
6. Holtzman R, Silin DB, Patzek TW. Mechanical properties of granular materials: a variational approach to grain-scale simulations. *International Journal for Numerical and Analytical Methods in Geomechanics* 2009; **33**(3):391–404, doi:10.1002/nag.725.
7. Holtzman R, Silin DB, Patzek TW. Frictional granular mechanics: a variational approach. *International Journal for Numerical Methods in Engineering* 2010; **81**:1259–1280, doi:10.1002/nme.2727.
8. Dvorkin J, Mavko G, Nur A. The effect of cementation on the elastic properties of granular material. *Mechanics of Materials* 1991; **12**(3):207–217.
9. Dvorkin J, Nur A, Yin H. Effective properties of cemented granular materials. *Mechanics of Materials* 1994; **18**(4):351–366.
10. Jin G, Patzek TW, Silin DB. Physics-based reconstruction of sedimentary rocks (SPE83587). *SPE Western Regional/AAPG Pacific Section Joint Meeting, 19–24 May, 2003.*, Long Beach, CA, 2003.
11. Delenne JY, El Youssoufi MS, Cherblanc F, Bénet JC. Mechanical behaviour and failure of cohesive granular materials. *International Journal for Numerical and Analytical Methods in Geomechanics* 2004; **28**(15):1577–1594, doi:10.1002/nag.401.
12. Potyondy DO, Cundall PA. A bonded-particle model for rock. *International Journal of Rock Mechanics and Mining Sciences* 2004; **41**(8):1329–1364, doi:10.1016/j.ijrmms.2004.09.011.
13. Johnson KL. *Contact Mechanics*. Cambridge University Press: Cambridge, MA, 1987.
14. Dvorkin J, Nur A. Elasticity of high-porosity sandstones: theory for two North Sea data sets. *Geophysics* 1996; **61**(5):1363–1370, doi:10.1190/1.1444059.
15. Holt RM. Particle vs. laboratory modelling of In Situ compaction. *Physics and Chemistry of the Earth (A)* 2001; **26**(1–2):89–93, doi:10.1016/S1464-1895(01)00028-X.
16. Nakagawa S, Myer LY. Mechanical and acoustic properties of weakly cemented granular rocks. *Technical Report LBNL-50814 (http://escholarship.org/uc/item/8926x469)*, Lawrence Berkeley National Laboratory, Berkeley, CA 2001.
17. Nakagawa S. Acoustic experiments on synthetic and natural weakly cemented sands 2008. Unpublished data.

18. Jaeger JC, Cook NGW. *Fundamentals of Rock Mechanics*. Third edn., Chapman and Hall: London, UK, 1979.
19. Holtzman R. Micromechanics of sediments: a variational approach to grain-scale simulations. PhD Thesis, University of California, Berkeley, CA 2008.
20. Kranz RL. Microcracks in rocks: a review. *Tectonophysics* 1983; **100**(1–3):449–480, doi:10.1016/0040-1951(83)90198-1.
21. Martin CD, Chandler NA. The progressive fracture of Lac du Bonnet granite. *International Journal of Rock Mechanics and Mining Sciences and Geomechanics Abstracts* 1994; **31**(6):643–659, doi:10.1016/0148-9062(95)96975-H.
22. Saidi F, Bernabè Y, Reuschlè T. Uniaxial compression of synthetic, poorly consolidated granular rock with a bimodal grain-size distribution. *Rock Mechanics and Rock Engineering* 2005; **38**(2):129–144, doi:10.1007/s00603-004-0040-5.
23. Mindlin RD, Deresiewicz H. Elastic spheres in contact under varying oblique forces. *Journal of Applied Mechanics* 1953; **20**:327–344.
24. Deresiewicz H. Contact of elastic spheres under an oscillating torsional couple. *Journal of Applied Mechanics* 1954; **21**:52–56.
25. Yin H, Dvorkin J. Strength of cementated grains. *Geophysical Research Letters* 1994; **21**(10):903–906.
26. Tavarez FA, Plesha ME. Discrete element method for modelling solid and particulate materials. *International Journal for Numerical Methods in Engineering* 2007; **70**:379–404, doi:10.1002/nme.1881.
27. Timoshenko SP, Goodier JN. *Theory of Elasticity*. 3rd edn., McGraw-Hill: New York, 1970.
28. Berge PA, Bonner BP, Berryman JG. Ultrasonic velocity-porosity relationships for sandstone analogs made from fused glass beads. *Geophysics* 1995; **60**(1):108–119, doi:10.1190/1.1443738.
29. Hilbert LB Jr, Hwong TK, Cook NGW, Nihei KT, Myer LR. Effects of strain amplitude on the static and dynamic nonlinear deformation of Berea sandstone. *Rock mechanics Models and Measurements Challenges from Industry*, Nelson PP, Laubach S (eds.). Balkema, Rotterdam, 1994; 487–504.
30. Zangerl C, Evans K, Eberhardt E, Loew S. Normal stiffness of fractures in granitic rock: A compilation of laboratory and in-situ experiments. *International Journal of Rock Mechanics and Mining Sciences* 2008; **45**(8):1500–1507, doi:10.1016/j.ijrmms.2008.02.001.